

Design and Implementation of RC Servo Motor Based Miniature Series Elastic Actuators

Chung-Wei Lee* and Jung-Hua Chou**

Keywords : actuator design, RC servo motor, miniaturized series elastic actuator, hopping.

ABSTRACT

This paper presents a novel design and implementation of a miniaturized series elastic actuator (SEA) with RC servo motor based mechatronic architecture using a rotary type elastic element. A pre-compressed and further stressed spring elastic element is applied to reduce torque noises and to decrease the control complexity. A non-invading modified servo design is used to cancel the internal RC servo motor controller by an inverse function method. An external cascaded controller is added to improve the control capability of the RC servo motor based SEA. Moreover, an oscillation controller is implemented to achieve cyclic dynamic motions such as hopping. Finally, the performance of the miniaturized SEA is demonstrated by the rotary load arm testing module and the ES-RC hopping leg module. The results show that the torque noise can be reduced to an acceptable level; the position and velocity tracking perform well. Further the hopping results show that the energy-storage property of series elastic actuator works well and an average hopping height of 16 mm can be achieved

INTRODUCTION

Series elastic actuators (SEAs) have been studied for many years. Various SEAs are proposed for different applications and control requirements. Differing from traditional rigid actuators, SEAs contain an elastic element in series with the mechanical energy source. Hence, SEAs have special properties provided by the elastic element, including better tolerance to impact load, increased peak power output, and passive mechanical energy storage (Pratt and Williamson, 1995; Arumugom et al., 2009; Paluska and Herr, 2006). On the other hand, in order to accomplish these unique properties, an appropriate design of the elastic element is necessary.

Paper Received May, 2020. Revised July, 2020. Accepted July, 2020. Author for Correspondence: Chung-Wei Lee.

* Graduate Student, Department of Engineering Science, National Cheng Kung University, Tainan, Taiwan, ROC.

** Professor, Department of Engineering Science, National Cheng Kung University, Tainan, Taiwan, ROC.

(2006) designed a compact, high-performance linear SEA. A linear spring is placed between the motor housing and the chassis ground. The SEA uses a piston-style ball screw mechanism which contains a concentric elastic element to achieve the compact size and lightweight not obtainable by previous ball screw SEA designs.

A rotary SEA is implemented based on off-the-shelf components, a planetary gearbox is applied for speed reduction, and the transmission of power output is through a bevel gear (Kong et al., 2009). The SEA is implemented with a rotary elastic element using a torsional spring. However, the design based on many commercially available components can be difficult to achieve a compact size.

Linear springs can also be used for rotary elastic element designs. As in “iCub” robot (Tsagarakis et al., 2009), the SEA is designed for satisfying the weight requirements. To minimize dimensions while achieving high rotary stiffness, a three-spoke output structure composed of a circular input pulley and six linear springs is applied in the rotary elastic element.

The high-stiffness custom torsional spring designs are applied in the rotary elastic elements to minimize weight and dimensions. A monolithic disc-shaped spring design (Sergi et al., 2012) and a double-spiral spring design (Lagoda et al., 2010) are implemented, respectively. Those designs allow the bulk reduction in the radial direction while still maintain the SEA thickness at an acceptable level.

Hutte et al. (2009) designed an SEA for a highly compliant robotic knee. The rotary elastic element composes of a pulley system in combination with a single pre-compressed spring. As a result, the spring characteristic is nonlinear during the rotation of knee joint.

In addition to fixed stiffness characteristics of elastic element designs, variable stiffness actuator design is introduced in CompAct-VSA (Tsagarakis et al., 2011a) by using a lever arm mechanism with a variable pivot axis. When the lever arm rotates around the pivot point, the linear springs generate an elastic force. The stiffness regulation is achieved by the movement of the pivot point with respect to the center of rotation of the CompAct-VSA joint.

For linear elastic element designs, the loading force of SEA can be measured by the distance of

spring deflection. And for rotary elastic element designs, the loading torque of SEA can be measured by the angle of spring deflection. Because the loading forces or torques of SEAs can be sensed readily during dynamic motion and special properties described above (Pratt and Williamson, 1995; Arumugom et al., 2009; Paluska and Herr, 2006), SEAs have been widely adopted in the fields of humanoid robotics, legged robotics and haptic laparoscopic devices.

The “cCub” compliant humanoid robot (Tsagarakis et al., 2011b) implements passive compliant actuation in the major joints of the leg based on the SEA principle. The robot exploits the characteristics of safer interaction, energy efficiency, and more aggressive damage-free learning.

A hydraulically actuated Quadruped robot (HyQ) is implemented with legs of hydraulic cylinder actuators driven by air (Semini et al., 2010; Ugurlu et al., 2013). The compressibility of air provides the actuator some degree of intrinsic compliance. The leg also contains a visco-elastic rubber coated foot to dampen out the impacts at touchdown. Hence the leg has SEA liked properties and is suitable for highly dynamic situations of legged robots.

A compliant quadruped robot calls cheetah-cub is presented (Sprowitz et al., 2013). Its leg configuration is based on a spring-loaded, pantograph mechanism with multiple segments. Each leg is actuated by two RC servo motors: the hip actuator is directly connected to the hip joint and the knee actuator drives the knee joint via a cable mechanism. The knee actuator retracts the leg by pulling the cable. On the other hand, leg extension is due to springs. That is, the cheetah-cub’s legs can be treated as a specific SEA design comprising RC servo motors, leg structures and series elastic elements.

The compliant quadruped robot, StarLETH (Hutter et al., 2012a; Hutter et al., 2012b; Hutter et al., 2013), is fully actuated with high compliant leg modules which are able to perform precise joint torque and position control so that the exploitation of natural dynamic motions can be fulfilled. To keep the leg inertial small, a weight-optimized drive unit containing harmonic drive gearboxes and two Maxon DC motors for hip and knee flexion/extension serves as the hip joint axis, and a robust chain drive with steel cable pulley connects the motor to a compression linear spring in the shank.

Garcia et al. (2011) designed biomimetic legs for agile quadrupeds are presented using the key principles of horse legs which are responsible for agile and powerful locomotion. The leg actuation system is based on the hybrid use of SEAs and magneto-rheological dampers to provide variable compliance for natural motion.

The legs of the spring-legged, monopod robot, ATRIAS 1.0 (Grimes and Hurst, 2012), are specifically designed according to called the Spring

Loaded Inverted Pendulum (SLIP) model which approximately describes the steady-state legged locomotion for most legged animals. For the robot, the large series springs are driven by two brushless DC motors via cable pulley mechanisms and the four-bar leg is actuated through the movement of large series springs.

Basafa et al. (2009) implemented a laparoscopic haptic device based on a 4-DOFs mechanism and SEAs. The invading modified RC servo motors are developed and used as the torque sources of SEAs.

In this paper, a novel miniaturized SEA based on RC servo motor is designed and implemented. In addition to this Section, the organization of this paper is as follows. The hardware design concept of ES-RC SEA (Engineering Science-Radio Control Series Elastic Actuator) is described, including motor, drivetrain and the pre-compressed and further stressed spring elastic element. Then the internal RC servo motor controller model, the non-invading modified servo design and the proposed control algorithm are illustrated. The performance of ES-RC SEA is evaluated by the rotary load arm test and the ES-RC hopping leg experiment.

HARDWARE DESIGN

The goal of the miniaturized SEA in this research is both compact size and light weight (lower than 100 g). Hence, the motor and drive train of the specially designed ES-RC SEA are selected. The prototype of ES-RC SEA, shown in Fig 1 is with length, width, height, and weight of 62 mm, 52 mm, 35 mm, and 55.8 g, respectively. Additionally, a pre-compressed and stressed spring structure is applied to the elastic element to minimize dimensions, reduce the torque sensor noise and decrease the control complexity.

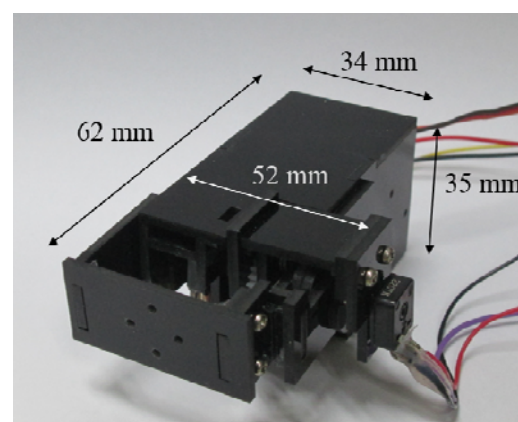


Fig.1. Hardware of ES-RC SE

Motor and drivetrain

In many small sized robots, RC servo motors are used as the mechanical energy source [19], [20]. RC servo motors have two important features for achieving a light weight, large torque, and miniaturized SEA design. Firstly, due to the requirements of radio control applications, compact sized gearboxes are particular manufactured and embedded in their limited space. Secondly, a simplified controller combining the motor driver with position controller is adopted as their internal controller. Because of popularity, a variety of possible selections of motor and drive train based on off-the-shelf RC servo motors is available.

On the other hand, RC servo motors have some disadvantages. Firstly, their position errors are influenced by the loading mass in most applications. These errors typically increase with heavier loading mass. Additionally, most RC servo motors have no speed control function due to the simplified internal controller even though this situation can be resolved practicably by the invading methods [20]. In this paper, a non-invading method of modified RC servo is proposed which will be described later.

The ES-RC SEA uses a RoBoard RS-0263 RC servo motor. As in Fig. 2, the RC servo motor actuates the gear shaft perpendicular to the RC servo motor shaft through a crown-gear train. This arrangement is for installing two potentiometers with minimized width for the ES-RC SEA. The potentiometer connected to gear shaft senses the information of the RC servo motor for the non-invading modified servo design. A rotary elastic element is put between the gear shaft and output shaft of the ES-RC SEA. The potentiometer placed outside the output shaft measures the conditions of the rotary elastic element.

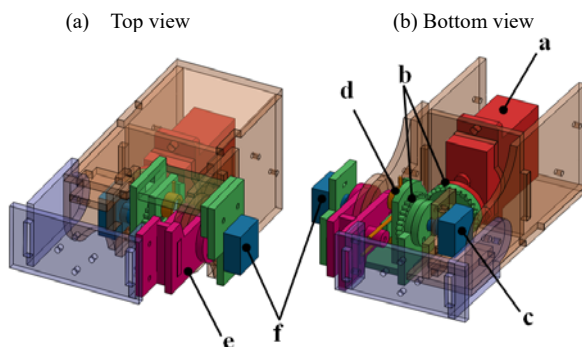


Fig. 2. Perspective views of ES-RC SEA showing the components of (a) RoBoard RS-0263 RC servo motor, (b) crown-gear train, (c) potentiometer connected with gear shaft, (d) rotary springs, (e) output shaft of ES-RC SEA, (f) potentiometer connected between gear shaft and output shaft.

Elastic element

The rotary type elastic element is adopted to save space. In the literature, various elastic element designs are available. In this paper, a pre-compressed spring structure design is used. The cross section of the elastic element is shown in Fig. 3. The motor shaft and the block are combined together where the block constrains two pre-stressed springs. If the loading torque exceeds the threshold torque (τ_{th}) of the pre-stressed spring, the ball bearing connected to the output shaft will push the spring to rotate the output shaft relative to the motor shaft, either clockwise or counterclockwise as shown in Fig. 4. If the loading force does not exceed τ_{th} , the output shaft will stay in its original position as in Fig. 3 and Fig. 4(b). The spring deflection angle (θ_d) is defined as the angle between the motor shaft and the output shaft.

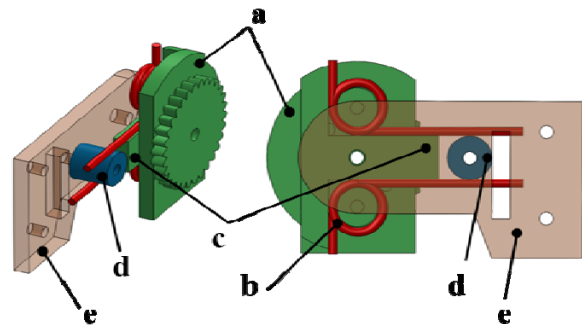


Fig. 3. Cross section of the elastic element: (a) gear shaft driven by RoBoard RC servo motor via the crown-gear train, (b) pre-compressed rotary spring, (c) the block and the pre-compressed springs, (d) ball bearing connecting the output shaft of SEA, (e) output shaft.

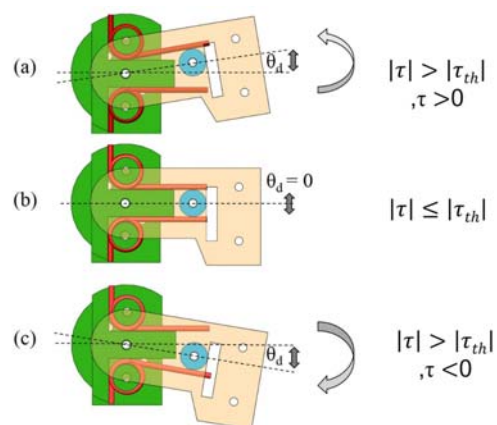


Fig. 4. Rotary motions of the elastic element: (a) counterclockwise rotation, (b) remaining at the original position, (c) clockwise rotation.

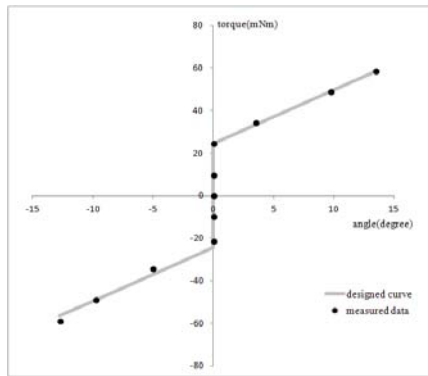


Fig. 5. Trends of measured and designed torque versus deflection angle.

From Hooke’s law, the spring deflection angle of the rotary elastic element is as follows:

$$\begin{cases} \theta_d = \frac{\tau - \tau_{th}}{k}, & |\tau| > |\tau_{th}|, \tau > 0 \\ \theta_d = 0, & |\tau| \leq |\tau_{th}| \\ \theta_d = \frac{\tau + \tau_{th}}{k}, & |\tau| > |\tau_{th}|, \tau < 0 \end{cases} \quad (1)$$

The spring deflection angle (θ_d) is calculated by dividing the difference between the spring torque (τ) and the torque threshold (τ_{th}) to the spring constant (k) as illustrated by equation (1). When $|\tau_{th}|$ is less than $|\tau|$, the spring torque is exerted by the loading impact and the torque threshold (τ_{th}) is induced by the stressed spring which is already pre-compressed by the block structure. Therefore, the contribution has to be removed in calculating the deflection angle. In contrast, when the $|\tau|$ is smaller than $|\tau_{th}|$, θ_d will be zero as the springs remain in their original pre-stressed positions.

Through the pre-stressed spring structure, torque noises of small amplitudes not exceeding the torque threshold can be suppressed. The threshold torque of the pre-compressed springs is designed and measured. It is 24.5 mN-m for the ES- R/C SEA. The relation between the spring deflection angle (θ_d) and the spring torque (τ) is measured and shown in Fig. 5. The linear relation is expected while the threshold is evident. Details of the ES-RC SEA are summarized in Table 1.

Table 1. ES-RC SEA specification

Specifications	Values
Weight	55.8g
Length	62 mm (output shaft not included)
Height	35 mm
Width	52 mm (max) ~ 34 mm (min)
Potentiometer to motor shaft	1 count/0.25deg
Potentiometer between motor shaft and output shaft	1 count/0.25deg
Measured spring constant K	2.8 mN-m/deg
Torque threshold of elastic element	24.5 mN-m

MODELING AND CONTROL

In general, position errors of RC servo motors are influenced by their loading mass. Moreover, most RC servo motors lack speed control because they use simplified internal controllers. This latter situation can be resolved by modifying the RC servo motor through invading methods as in [20] for a laparoscopic haptic device. However, in that case, the RC servo modified by the invading method cannot be recovered. To avoid this situation, a non-invading modified servo design is taken in this study by measuring the transfer function of the R/C servo controller first. Then, an inverse function method is applied to cancel the original internal controller so that the internal controller can be replaced with a desired external controller as follows.

Modeling and non-invading modified Servo design

A typical control system diagram of an RC servo motor with an internal controller is shown in Fig. 6 where r and y are the input reference and output positions of the motor, respectively. The position error e between r and y is measured by the internal potentiometer. The error is fed to the RC servo controller with the transfer function G . The output u from the servo controller is input to the servo motor control plant P to obtain the current output position y which is compared to the reference position r to obtain position error e .

The transfer function G can be obtained by measurements as follows. By ignoring the transient behavior of G and fixing the internal potentiometer of the RC servo motor to zero, the position error (e) is determined by the reference r first. The RC servo controller output u is the pulse-width-modulated (PWM) signal used to efficiently modulate the voltage applied to the RC servo motor. The duty ratio of the PWM signal, measured by an oscilloscope, represents the percentage of power applied to the R/C servo motor. Then, the transfer function G is deduced by dividing the position error e to the RC servo controller output u . Fig. 7 depicts the measured result of u versus e . By curve fitting through the measured data, steady state G is obtained.

After obtaining G from above, the present non-invading modified servo design is achieved by cancelling the original RC servo controller by the inverse of G , namely G^{-1} as shown in the left portion of Fig. 8. For this situation, the output y is measured by an external potentiometer and is added to the system to cancel the measured y obtained from the internal potentiometer. Because G^{-1} multiplied by G is 1, the equivalent system block diagram illustrated in the right portion of Fig. 8 shows that r simply equals to u . Hence, the input reference r is equal to output u after applying the inverse function method. To confirm the validity of this method for the original RC servo control system, a test of power linearity is conducted. In the test, the internal and external

potentiometers measure the same y while inputting the desired power percentage to the system and measuring the output power percentage by an oscilloscope. Fig. 9 shows the test results and the linearity is remarkable as expected.

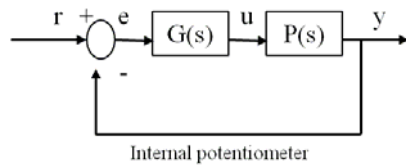


Fig. 6. Block diagram of R/C servo control system.

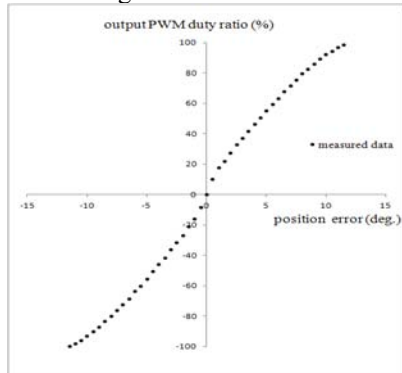


Fig. 7. Relation between u and e of the original RC servo controller.

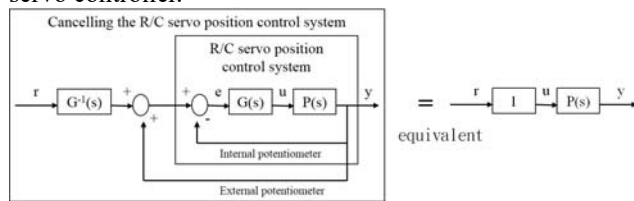


Fig. 8. Concept of the inverse function method.

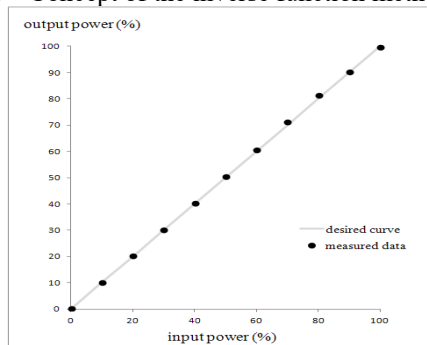


Fig. 9. Result of power linearity test.

Cascaded controller

By implementing the non-invasive modified servo design, using the inverse function method described above, the performance improvement of the RC servo motor for robotic manipulators can be realized by adding an external controller. In this regard, some cascaded controller architectures are developed for position and velocity controls. In this study, the proposed cascaded controller scheme is as Fig. 10. The inner loop of the controller scheme is the velocity control loop which consists of a PI controller.

The output of the PI controller is fed into the cancelled RC servo controller by the inverse function method. The outer loop is the position control loop. The position command is executed by saturating the saturation function to a desired velocity before entering the inner loop. Hence, the ES-RC SEA can move the output shaft to a desired position with a desired velocity.

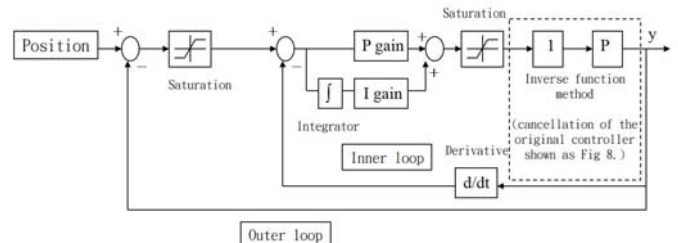


Fig. 10. Proposed cascaded controller scheme.

Oscillation controller

Differing from of robotic manipulator applications, the cyclic dynamic motion such as hopping requires motion control with a desired period. For the ES-RC SEA, the dynamic motion is expected due to the energy-reusable characteristic of SEAs. During the dynamic motion, the actuators have impact loads for which the SEAs can storage energy, and release it later. To control the cyclic dynamic motions, an oscillation algorithm is applied.

During the oscillation process, the power of the ES-RC SEA is set to maximum. The oscillation control algorithm consists of a PI controller for adjusting the amplitude of oscillation which in turn controls the oscillation period because of the fixed power of the ES-RC SEA. As shown by the control flow chart illustrated in Fig. 11, the first step of the algorithm is to detect the oscillation boundary until the ES-RC SEA reaches the oscillation boundary which is determined by the output amplitude. After reaching the position boundary, the actual oscillation period is calculated. Then, the PI controller is used to decide the next output amplitude. As oscillation is a reciprocating motion, the ES-RC SEA actuates reversely with the maximum power in the next step. Finally, the process returns to the first step and repeats the entire flow of the oscillation control algorithm. By this algorithm, the ES-R/C SEA can produce a cyclic dynamic motion such as hopping with a desired period.

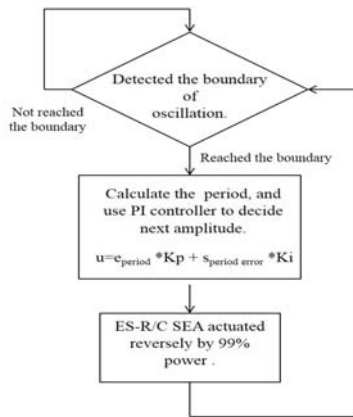


Fig. 11. Flow chart of the oscillation control algorithm (e_{period} : error of period, $s_{period error}$: sum of period error, K_p : P gain, K_i : I gain, u : next amplitude).

EXPERIMENTS AND DISCUSSION

The performance of those two controller architectures described above is checked by experiments in three phases. The first phase is to verify the position and velocity accuracy of the ES-RC SEA cascaded controller. The second phase is to test the oscillation control algorithm. The last phase is a cyclic dynamic motion test using the ES-RC hopping leg which is actuated by the implemented ES-RC SEA by measuring the performance of the actual actuator. The results of these experiments confirm the energy-reusable characteristic. Details are as follows.

Position and velocity test

The position and velocity performance of the cascaded controller is tested by a loaded rotary arm as in Fig. 12. The arm contains a counterweights used as the rotary load and the ES-RC SEA is mounted on the base of the arm module. The rotary load resembles the load of a robotic manipulator. In the testing, both desired position and velocity are set for the actuator to track them. For the rotary load arm test, four designed velocities of 75, 125, 200, and 250 degrees/sec are included with same position traveling range from 15 to 65 degrees and same load of 0.05 kg in weight on the 0.05 m moment arm. The position and velocity trajectories of test are shown in Figs. 13 and 14, respectively. From the results shown in Fig. 13, the measured position trajectories of the ES-RC SEA through the cascaded controller are close to the desired trajectories. That is, position tracking by the cascaded controller performs successfully for the four velocities tested.

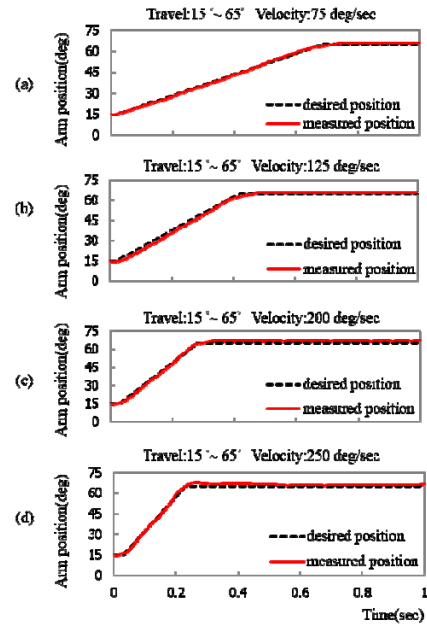


Fig. 13. Position trajectories of four velocities: (a) 75 degrees/sec, (b) 125 degrees/sec, (c) 200 degrees/sec, (d) 250 degrees/sec.

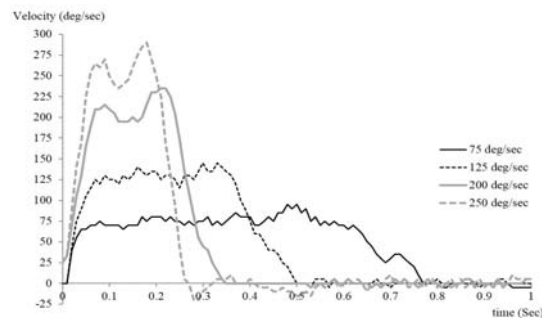


Fig. 14. Velocity trajectories of velocities 75, 125, 200, and 250 deg/sec with the same goal position of 65 degrees.

Further, from the positions measured by the external potentiometer, the velocity trajectories can be calculated by differentiation the position trajectories with respect to time. In this study, the velocity resolution calculated by this method is 25 degrees/sec. In order to reduce the associated error, a five-point moving average is performed in obtaining the velocity trajectories. The results are shown in Fig. 14. It can be observed that the trends of four velocity trajectories are the same. That is, from the beginning, the actuator speeds up the velocity to the desired value first. Then it keeps the velocity at the desired value until the goal position of the rotary arm is approached. Afterwards, the actuator speed slows down to zero. When the actuator remains at desired velocities, some ripples occur in the steady-state of velocity trajectories. These ripples are larger for higher desired velocities and may be caused by numerical differentiation due to lack of velocity resolution and the neglect of the transient behavior in the model of the original RC servo controller.

The performance errors of the cascaded controller of the above experiments are summarized in Table II. The average steady-state errors of position are obtained from the position trajectories shown as Fig. 13. And the average steady-state errors of velocity are calculated from the slopes of position trajectories at the stages of remaining the desired velocities. For the four testing conditions, the averages of steady-state errors in position and velocity are lower than 3 % and 5 %, respectively. Hence, the performance of the cascaded controller is acceptable. Moreover, improving the performance of RC servo motor by the non-invading modified servo design is also confirmed.

Table 2. Position and velocity test results

Goal of Velocity	Goal of Position	Average of Position Steady-State error	Average of Velocity Steady-State error
75 (deg/sec)	65	1.9 (%)	2.4 (%)
125 (deg/sec)	65	1.2 (%)	2.8 (%)
200 (deg/sec)	65	2.7 (%)	4.2 (%)
250 (deg/sec)	65	1.7 (%)	3.2 (%)

For all the rotary arm tests described above, the ES-RC SEA adopts the elastic element with the pre-compressed and further stressed spring structure. The proposed and implemented elastic element can effectively reduce the torque noise of the rotary arm motion by the torque threshold. The comparisons of position trajectories and torque noise trajectories with and without the proposed elastic element are depicted in Fig. 15 using the same load of 0.05 kg in weight on the 0.05 m moment arm. The results illustrate that the position trajectory without torque threshold is not satisfactory at all in tracking the desired position whereas the one with torque threshold tracks well. Similarly, with torque threshold, the torque noise is close to zero in contrast to the large noise associated with the one without torque threshold. That is, the proposed elastic element design works successfully.

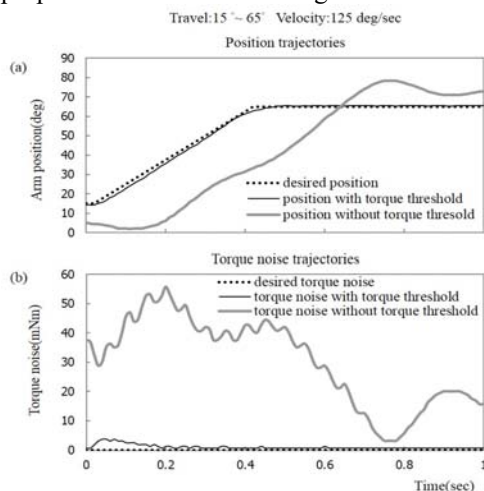


Fig. 15. Comparisons of position and torque noise trajectories for cases with and without torque threshold.

Oscillation experiments

The oscillation control algorithm is designed for producing a cyclic dynamic motion such as hopping with a desired period. Before taking the hopping leg experiment, the oscillation experiments are conducted for confirming the performance of oscillation controller, using the rotary load of 0.02 kg and moment arm of 0.05 mm. The cyclic oscillation experimental results are given in Fig. 16 for the periods of 300 ms and 200 ms. From the trajectories of cyclic oscillation period shown in Fig. 16, the range of period steady-state errors is about ± 20 ms due to the measurement resolution of 10 ms imposed by the sampling rate of oscillation controller. On the other hand, the average measured period matches the desired period very well. Hence, the control algorithm performs acceptably.

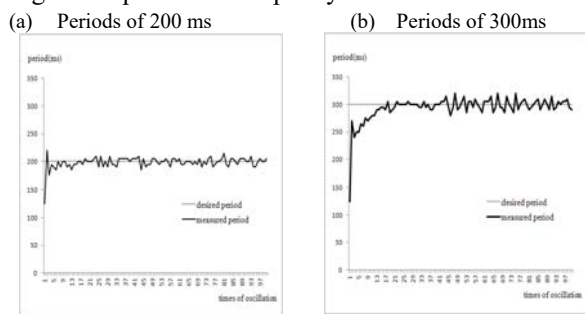


Fig. 16. Cyclic oscillation results.

Hopping leg experiment

After confirming the oscillation controller, hopping leg experiments are conducted to evaluate the energy storage characteristics of the actuator by a special designed hopping module. The module consists of a robotic leg, called ES-RC Hopping Leg, mounted with the ES-RC SEA as shown in Fig. 17. The ES-RC Hopping Leg (circled in Fig. 17) is a 1-D hopping motion leg. The leg is connected to a base via a rotary linkage. Counter weights are mounted to the opposite side of the leg structure. During the hopping motion, the leg hops while the linkage rotates. Details of the hopping leg shown in Fig. 18 illustrate that the ES-RC SEA drives the knee joint via the output shaft connected to the leg mechanism. The oscillation algorithm described above is applied for achieving the cyclic oscillation of the leg.

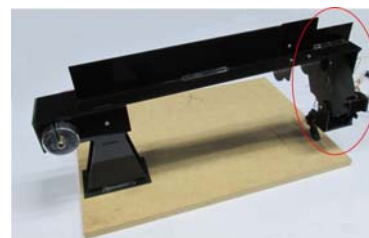


Fig. 17. Bird-eye view of ES-RC hopping leg

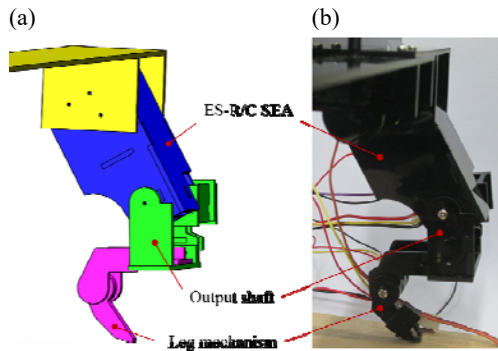


Fig. 18. Lateral view of hopping leg: (a) Schematic drawing; (b) Real.

Some snapshots of the hopping motion of the ES-RC hopping leg are showing in Fig. 19. The hopping leg starts the hopping motion by squatting down first as shown in Fig. 19(a). Then the knee joint of the ES-RC hopping leg, being driven by the ES-RC SEA, swings back and forth quickly, so that the leg lifts off ground surface as illustrated in Figs. 19(b) and 19(c). Finally, as shown in Fig. 19(d), the hopping leg lands and completes one cycle of the hopping motion.

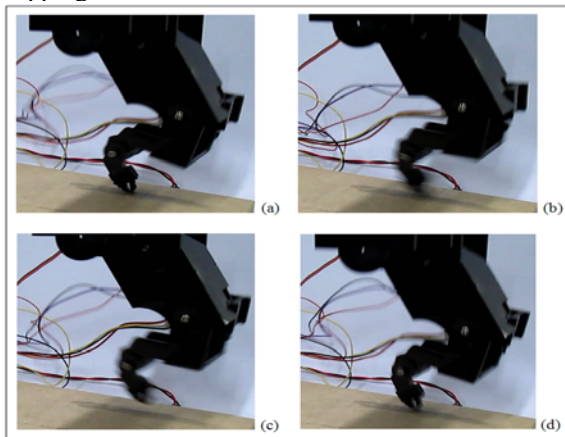


Fig. 19. Snapshots of hopping motion of the hopping leg.

The results of the hopping leg experiment are shown in Fig. 20. The SEA motor shaft of rotates back and forth from 42 degrees to 69 degrees with average oscillation period of 170 ms as Fig. 20(a). The SEA energy storage characteristics as illustrated in Fig. 20(b) can be observed through the torque trajectory measured by the elastic element. The torque trajectory has a DC offset due to the torque threshold imposed on the elastic element. During the impact of the leg with the ground, the elastic element receives an impact torque larger than the threshold torque and the SEA stores the associated energy and releases it later via the elastic element. The heights of hopping motion can be calculated by the measured information of each rotary joint as shown in Fig. 20(c) exhibiting periodic variations. The average hopping height is about 16 mm.

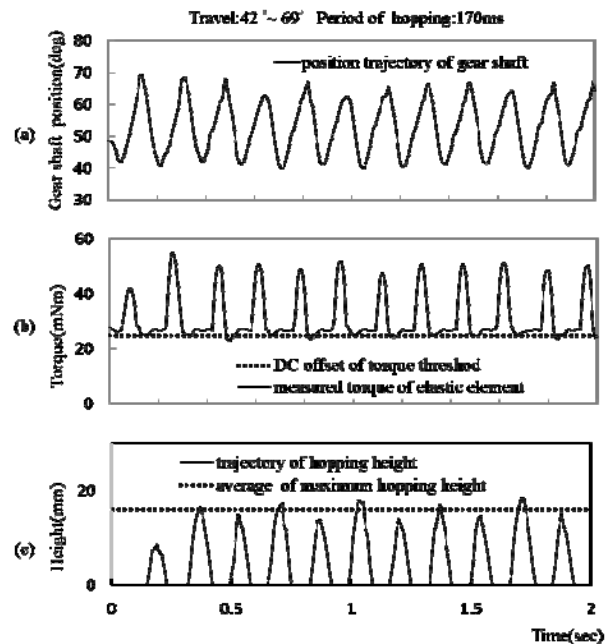


Fig. 20. Results of hopping experiment.

CONCLUSIONS

This paper realizes an RC servo based miniaturized SEA in three stages. Firstly, for the requirements of a miniature actuator design, a RC servo motor based SEA is designed and implemented with a specific design rotary elastic element. Next, a non-invasive modified servo design is introduced that cancels the internal RC servo motor controller by using inverse function method, and the external controllers added to improve the performance of actuator in applications of manipulator and hopping motion. Lastly, the miniature series elastic actuator's performance is demonstrated through experiments.

Key conclusions as follows:

1. The miniaturized SEA with 62 mm in length, 52 mm in width, 35 mm in height, and light weight of 55.8 g has been designed and implemented successfully by using off-the-shelf RC servo motors and incorporating a pre-compressed and further stressed rotary elastic spring element.
2. The torque noise is reduced greatly to an acceptable level by applying a torque threshold.
3. A cascaded controller is designed for position and speed control using an inverse function method and a non-invasive modified servo design. Verification results by the rotary arm testing module confirms the desirable performance of the SEA with the average steady-state errors of position and velocity lower than 3% and 5%, respectively.
4. An ES-RC hopping leg has been designed and implemented for hopping motion through the oscillation controller for cyclic dynamic motion.

The energy-storage characteristic of the SEA has been observed during the impact landing of the leg. It demonstrated that during impact landing the SEA stores the associated energy and release it later via the elastic element successfully. Further, the average hopping height achievable is about 16 mm

The present pre-compressed and further stressed spring structure is implemented by setting a torque threshold of the elastic element. In the future, a nonlinear stiffness elastic element may be developed based on the proposed structure to remove the need of the torque threshold while still minimizing torque noises to an acceptable level. Additionally, the transient of the internal RC servo controller modeling presently ignored will be considered to improve the controllabilities of the internal RC servo controller.

REFERENCES

- Arumugom, S., Muthuraman, S. and Ponselvan, V., "Modeling and application of series elastic actuators for force control multi legged robots," *J. Comput.*, vol. 1, no. 1, pp. 26–33, Dec. (2009)
- Basafa, E., Sheikholeslami, M., Mirbagheri, A., Farahmand, F. and Vossoughi, G. R., "Design and implementation of series elastic actuators for a haptic laparoscopic device," *Engineering in Medicine and Biology Society, 2009. EMBC 2009. Annual International Conference of the IEEE*, pp. 6054 - 6057. (2009)
- Garcia, E., Arevalo, J.C., Muñoz, G., and Gonzalez-de-Santos, P., 2011. "On the Biomimetic Design of Agile-Robot Legs." *Sensors* 11, no. 12: 11305-11334. (2011)
- Grimes, J.A. and Hurst, J.W., "The Design of ATRIAS 1.0 a Unique Monopod, Hopping Robot," *International Conference on Climbing and Walking Robots (CLAWAR)*, July 2012. (2012)
- Hutter, M., Remy, C. and Siegwart, R., "Design of an Articulated Robotic Leg with Nonlinear Series Elastic Actuation", *Proc. of The 12th International Conference on Climbing and Walking Robots and the Support Technologies for Mobile Machines (CLAWAR)*, September 2009, 645-652. (2009)
- Hutter, M., Gehring, C., Bloesch, M., Hoepflinger, M., Remy, C.D. and Siegwart, R., "StarLETH: A Compliant Quadrupedal Robot for fast, efficient, and versatile Locomotion", *Proc. of the International Conference on Climbing and Walking Robots (CLAWAR)*, 2012.(2012a)
- Hutter, M., Hoepflinger, M., Gehring, C., Bloesch, M., Remy, C.D. and Siegwart, R., "Hybrid Operational Space Control for Compliant Legged Systems", *Proc. of the 8th Robotics: Science and Systems Conference (RSS)*, 2012. (2012b)
- Hutter, M., Remy, C., Hoepflinger, M.A. and Siegwart, R., "Efficient and Versatile Locomotion with Highly Compliant Legs", *IEEE/ASME Transactions on Mechatronics*, Vol. 18, No. 2, April 2013, 449-458. (2013)
- Kong, K., Bae, J. and Tomizuka, M., "Control of rotary series elastic actuator for ideal force-mode actuation in human-robot interaction applications," *IEEE/ASME Trans. Mechatronics*, vol. 14, no. 1, pp. 105–118, Feb. (2009)
- Lagoda, C., Schouten, A., Stienen, A., Hekman, E. and Kooij, H., "Design of an electric series elastic actuated joint for robotic gait rehabilitation training," in *Proc. IEEE 3rd RAS and EMBS Int. Conf. Biomed.Robot. Biomechatron.*, Sep. 2010, pp. 21–26. (2010)
- Ng, K.H., Yeong, C.F., Su, E.L.M. and Husain, A.R., "Implementation of cascade control for wheeled mobile robot straight path navigation," *Intelligent and Advanced Systems (ICIAS)*, 2012 4th International Conference, vol.2, pp. 503 - 506, Kuala Lumpur. (2012)
- Paine, N., Oh, S. and Sentis, L., "Design and Control Considerations for High-Performance Series Elastic Actuators," *IEEE/ASME Transactions on Mechatronics*, Volume: PP, Issue: 99, pp. 1-12. (2013)
- Paluska, D. and Herr, H., "Series elasticity and actuator power output," in *Proc. IEEE Int. Conf. Robot. Autom.*, May 2006, pp. 1830–1833. (2006)
- Pratt, G. and Williamson, M., "Series elastic actuators," in *Proc. IEEE/RSJ Int. Conf. Intell. Robot. Syst. Human Robot Interact. Cooper. Robot.*, Aug.1995, vol. 1, pp. 399–406. (1995)
- Semini, C., Tsagarakis, N.G., Guglielmino, E. and Caldwell, D.G., "Design and Experimental

Evaluation of the Hydraulically Actuated Prototype Leg of the HyQ Robot," IEEE/RSJ Int. Conf. on Intelligent Robots and Systems (IROS). (2010)

Sergi, F., Accoto, D., Carpino, G., Tagliamonte, N.L. and Guglielmelli, E., "Design and characterization of a compact rotary Series Elastic Actuator for knee assistance during overground walking," Biomedical Robotics and Biomechanics (BioRob), 2012 4th IEEE RAS & EMBS International Conference on, pp. 1931-1936, Rome, 24-27 June. (2012)

Sprowitz, A., Tuleu, A., Vespignani, M., Ajallooeian, M., Badri, E. and Ispeert, A.J., "Towards Dynamic Trot Gait Locomotion-Design, Control and Experiments with Cheetah-cub, a Compliant Quadruped Robot," The International Journal of Robotics Research 0278364913482017, first published June 17. (2013)

Tsagarakis, N.G., Laffranchi, M., Vanderborght, B. and Caldwell, D.G., "A Compact Soft Actuator Unit for Small Scale Human Friendly Robots," Proc. of IEEE ICRA 2009, pp4356-4362. (2009)

Tsagarakis, N.G., Sardellitti, I. and Caldwell, D.G., "A new variable stiffness actuator (CompAct-VSA): Design and modelling," in Proc. IEEE/RSJ Int. Conf. Intell. Robot. Syst., Sep. 2011, pp. 378-383. (2011a)

Tsagarakis, N.G., Li, Z., Saglia, J. and Caldwell, D.G., "The design of the lower body of the compliant humanoid robot "cCub", Robotics and Automation (ICRA), 2011 IEEE International Conference on, pp. 2035 - 2040, 9-13 May. (2011b)

Ugurlu, B., Havoutis, I., Semini, C. and Caldwell, D.G., "Dynamic Trot-Walking with the Hydraulic Quadruped Robot - HyQ: Analytical Trajectory Generation and Active Compliance Control," IEEE/RSJ International Conference on Intelligent Robots and Systems (IROS). (2013)

基於遙控伺服馬達之微型 串聯彈性致動器研製

李崇璋 周榮華
國立成功大學工程科學系

摘要

本文旨在介紹一種採用旋轉彈性元件且基於 RC 伺服馬達機電一體化架構設計所實現的微型串聯彈性致動器 (SEA)。應用預壓縮和進一步受壓的彈簧彈性元件以減少扭矩雜訊並降低控制複雜性。採用非侵入式改進伺服馬達設計，通過反函數法消除內部 RC 伺服馬達控制器之影響。並添加了一個外部串接控制器以提高基於 RC 伺服馬達之 SEA 的控制能力。此外實作出一個振盪控制器來實現循環動態運動，例如跳躍。最終通過旋轉負載臂測試模組和 ES-RC 機器腳展現了微型化 SEA 的性能。實驗結果表明，扭矩雜訊可以降低到可接受的水平；位置和速度跟踪表現良好。進一步的跳躍實驗結果顯示了串聯彈性致動器的儲能性能很好，平均跳躍高度可以達到 16 mm。